NUMERICAL SIMULATION OF BREAKING WAVES AND WAVE LOADING ON A SUBMERGED CYLINDER

Deborah Greaves
Department of Architecture and Civil Engineering, University of Bath, Claverton Down, Bath BA2 7AY U.K.
e-mail: d.m.greaves@bath.ac.uk

Introduction

When considering numerical simulation of extreme wave loading on floating offshore wave energy devices it is important that the model should include both viscous effects and wave breaking. This usually means solving the Navier Stokes or RANS equations together with a two-fluid interface capturing approach, such as level set or volume of fluid (VoF), in which the fluid dynamics equations are solved both in the air and water. Recent advances in development of high resolution advection schemes for the interface mean that some of the previous disadvantages of these methods, such as interface smearing, have been overcome (see e.g.Ubbink, 1997).

In this work, adaptive hierarchical grids are applied to simulation of viscous free surface waves over a submerged cylinder in a stationary tank and to breaking waves in a periodic domain. The Navier-Stokes equations are discretised using finite volumes with collocated primitive variables and solved using an operator splitting algorithm. A VoF approach is used for the evolving free surface, with a high resolution interface capturing scheme for advection of the interface. The equations are solved on adapting quadtree grids combined with Cartesian cut cells (Causon *et al*. 2000) and the methodology is described in detail by Greaves (2006).

Wave loading on a submerged cylinder

A submerged cylinder of diameter d = 0.2h, where h is the mean depth of liquid in the tank, is positioned at the horizontal centre of a unit square tank at depth 0.5h below the liquid surface. The liquid is given an initial cosine wave elevation, $\eta = a\cos(2\pi x/b)$, where x is measured along the length of the tank, b is the length of the tank and a = 0.02h is the wave amplitude. The fluid Reynolds number for the wave, $\mathrm{Re} = h\sqrt{gh}/\upsilon$ = 200. The quadtree grid has maximum division level equal to 7 and minimum division level (background grid resolution) equal to 5 (7x5 quadtree grid). A refinement band of 10 cells is maintained around the cylinder boundary as well as the interface and the grid adapts dynamically to maintain this interface band at each time step.

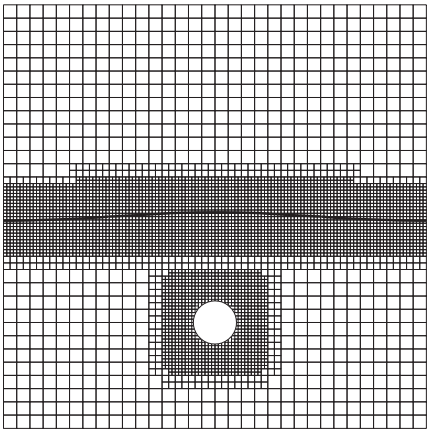

Figure 1 Free surface and adapted grid, cosine wave

The adapted grid at the first peak is shown in Figure 1 and the time history of the wave recorded at the centre of the tank is plotted in Figure 2 together with the wave-only case for comparison. The effect of the submerged cylinder is to dampen and cause a slight time lag in the wave motion at the free surface. The force on the cylinder is calculated by integrating the pressure and viscous shear stress around the cylinder and recorded at each time step. The hydrostatic force is

subtracted from the vertical force component and the hydrodynamic forces plotted in dimensional form in Figure 3.

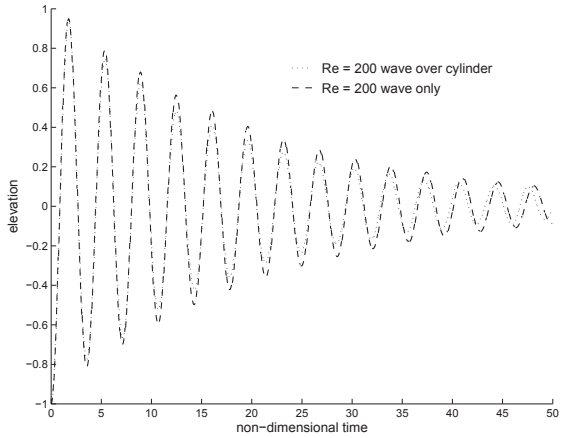

Figure 2 Wave elevation time history at the centre of the tank, Re=200 cosine wave

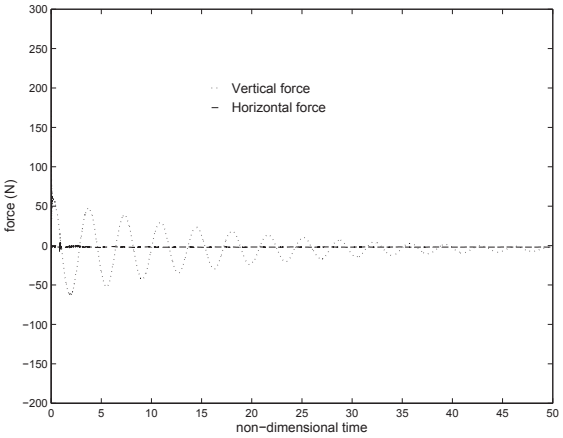

Figure 3 Time history of forces on submerged cylinder, Re = 200 cosine wave

The horizontal force is approximately zero, the vertical force is much larger and oscillates with the same frequency as, but exactly 180^o out of phase with, the wave motion. Considering the fluid kinematics under the centre of the symmetric cosine wave, the velocity is mainly in the vertical direction and so the vertical force is the in-line force. The phase of the vertical hydrodynamic force suggests that it is dominated by the inertia of the accelerating fluid. It is maximum when the vertical fluid acceleration is maximum at the troughs of the wave motion, and minimum when the acceleration is a minimum at the wave peaks. This is to be expected for cases such as this, in which the amplitude of the motion is small compared with the diameter of the cylinder (Bearman *et al.* 1985).

In the next case, the fluid Reynolds number for the wave, Re = 200, $a = 0.02h$ and the liquid is given an initial sine wave elevation, $\eta = a\sin(2\pi x/b)$. The cylinder is submerged at depth $0.25h$, as above, and the adapted grid and free surface profile after half a wave period are shown in Figure 4. The wave elevation time history at $x = b/4$ is plotted in Figure 5 and the horizontal and vertical hydrodynamic forces (with hydrostatic component subtracted) are presented in Figure 6.

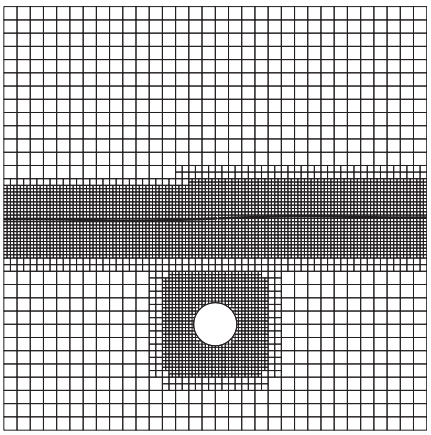

Figure 4 Free surface and adapted grid, sine wave

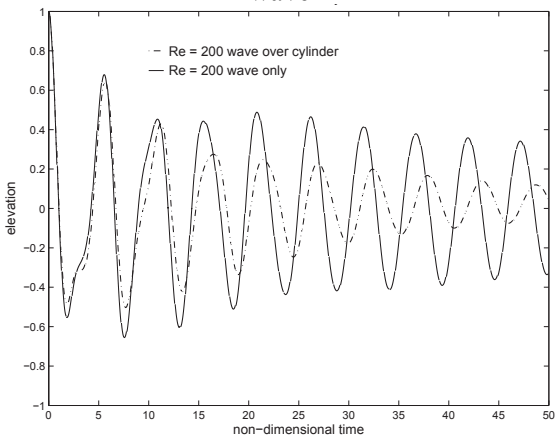

Figure 5 Wave elevation history at x=b/4, Re = 200 sine wave

Wave damping caused by the cylinder is stronger in this case and the wave frequency

is also reduced, as noted above. The undisturbed sine wave is asymmetric and at the cylinder position the horizontal velocity oscillates and the vertical velocity is approximately zero, thus, in this case, the in-line force on the cylinder is the horizontal force. This is shown in Figure 6, where after an initial disturbance the vertical force tends to approximately zero and the horizontal force oscillates with the same frequency and in phase with the wave motion recorded in Figure 5. As before, the horizontal force is mainly due to fluid inertia; when the wave peak is at $x = b/4$, the horizontal fluid acceleration (and horizontal force) at the cylinder is maximum, and when the wave trough is at $x = b/4$, the acceleration (and horizontal force) is at its minimum.

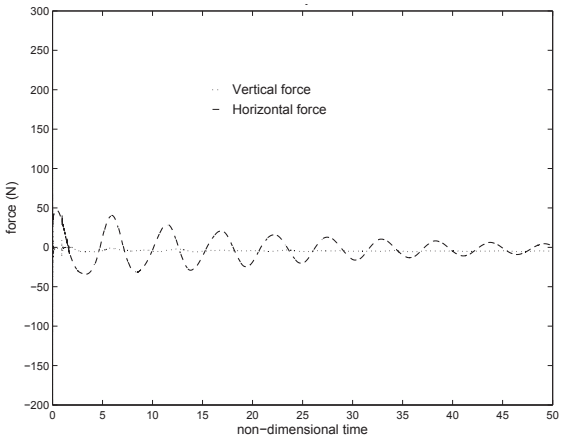

Figure 6 Time history of forces on submerged cylinder under a sine wave, Re = 200

Wave breaking in a periodic domain

A steep gravity water wave is simulated in a domain with periodic boundary conditions. The fluid properties and initial conditions are the same as those used by Chen *et al*. (1999) and Iafrati (2006). The width of the domain is one wavelength, $b =$, and the water depth is $h = b/2$. The ratio of density in air and water is 0.01 and the ratio of dynamic viscosities is 0.4. The initial condition for the wave elevation, is

$$\eta(x,0) = a\cos(kx) + \frac{1}{2}a^2 k\cos(2kx) + \frac{3}{8}a^3 k^2\cos(3kx)$$

where $k = 2\pi/\lambda$, a is the wave amplitude and the initial wave slope $\varepsilon = ak = 0.55$. The initial velocity field in the water is

$$u(x,y,0) = \omega a e^{ky}\cos(kx) \text{ and}$$

$$v(x,y,0) = \omega a e^{ky}\sin(kx),$$

where $\omega = \sqrt{gk(1-k^2a^2)}$ and the air is initially at rest. The acceleration due to gravity, $g = 1.0\text{m/s}^2$ and the liquid Reynolds number, $Re = \left(g^{1/2}\lambda^{3/2}/\upsilon\right)_l = 1000$. The simulation is calculated on a regular 256 x 256 grid.

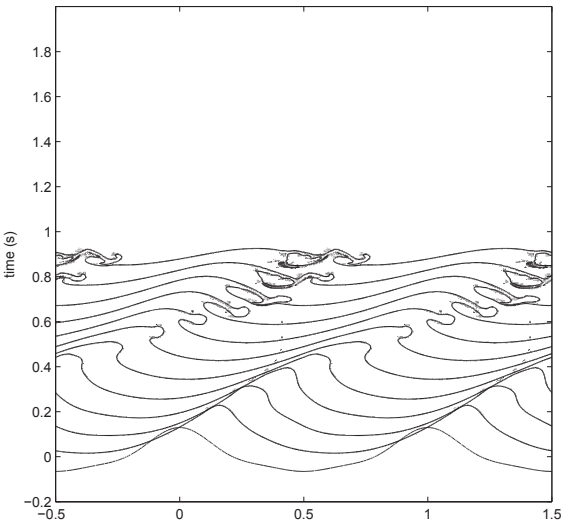

Figure 7 Time sequence of wave profiles

The time sequence of free surface profiles are illustrated in Figure 7, the profiles are plotted with the mean water level at their simulation time in seconds in the vertical direction and a second wavelength is plotted on the right hand side of each to clarify the figure. The steepening of the wave and development of a plunging jet is clearly seen. The jet makes contact with the free surface, entraining air, and then splashes up and makes contact again with the free surface entraining a second air pocket. Further splashing up of the jet to begin entraining a

third air pocket may be seen beyond this. Similar effects were observed in numerical calculations by Iafrati (2006) and Chen *et al*. (1999) and in photographs of experiments by Rapp and Melville (1990).

Individual free surface profiles are given in Figures 8 and 9 at non-dimensional times, $\tau = t/\sqrt{\lambda/g} =$ 0.56 and 1.76, together with the velocity vectors plotted every 16 cells. The velocity fields are visually similar to those predicted by Chen *et al.* (1999) and measured by Perlin *et al.* (1996) with features evident, such as the high velocities in the prominent jet. However, there are also some differences, such as the more rounded jet and slower progression to breaking predicted here.

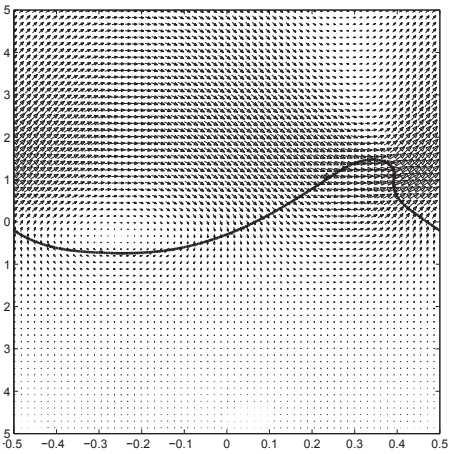

Figure 8 = 0.56

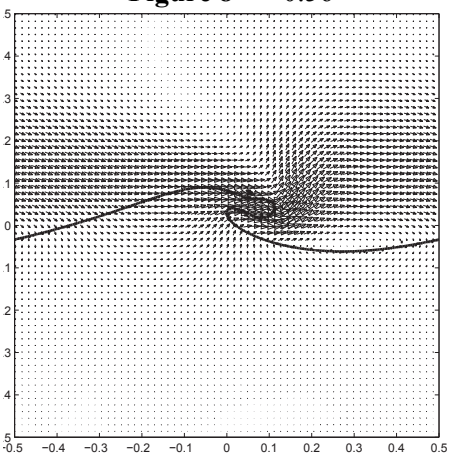

Figure 9 = 1.76

Conclusions

This new two-fluid Navier-Stokes solution method, using adaptive quadtree grids combined with Cartesian cut cells shows good potential for simulating violent interactions between waves and offshore structures. The method can predict complex deformation and break up of the free surface as well as detailed flow kinematics and fluid loading on structures.

Acknowledgements

The author is very grateful to the Royal Society for supporting this work through a Royal Society University Research Fellowship.

References

Bearman, P.W., Downie, M.J., Graham, J.M.R. and Obasju, E.D. 1985 Forces on cylinders in viscous oscillatory flow at low Keulegan-Carpenter numbers, *J. Fluid Mechanics*, 154, 337 – 356.

Causon, D.M., 2000 Calculation of shallow water flows using a Cartesian cut cell approach, *Advances in Water Resources,* **23**(5), 545-562.

Chen, G. Kharif, C., Zaleski, S. and Li, J. 1999 Two-dimensional Navier-Stokes simulation of breaking waves, *Physics of Fluids*, 11, 121 – 133.

Greaves, D.M. 2006b Viscous waves and wave-structure interaction in a tank using adaptive quadtree grids, *Journal of Fluids and Structures*, submitted.

Iafrati, A. 2006 Effect of the wave breaking mechanism on the momentum transfer, 21st International Workshop on water wave and floating bodies, Loughborough, 2-5 April 2006.

Perlin, M., He, J. and Bernal, L.P. 1996 An experimental study of deep water plunging breakers, *Physics of Fluids*, 8, 2365–2374.

Rapp, R.J. and Melville, W.K. 1990 Laboratory measurements of deep-water breaking waves, *Phil. Trans. Royal Society London, Series A,* 331:1622, pp. 735 – 800.

Ubbink, O. 1997 Numerical prediction of two fluid systems with sharp interfaces, PhD Thesis, Imperial College of Science, Technology and Medicine, London.